ASN NEURO RESEARCH ARTICLE

ASN NEURO 4(2):art:e00077.doi:10.1042/AN20110063

Regional and cell-type-specific effects of DAMGO on striatal D1 and D2 dopamine receptor-expressing medium-sized spiny neurons

Yao-Ying Ma*[1], Carlos Cepeda[†], Payush Chatta*, Lana Franklin*, Christopher J Evans* and Michael S Levine[†2]

*Stefan & Shirley Hatos Center for Neuropharmacology, David Geffen School of Medicine, University of California Los Angeles, Los Angeles, CA, U.S.A.

[†]Intellectual and Developmental Disabilities Research Center, David Geffen School of Medicine, University of California Los Angeles, Los Angeles, CA, U.S.A.

Cite this article as: Ma Y-Y, Cepeda C, Chatta P, Franklin L, Evans CJ and Levine MS (2012) Regional and cell-type-specific effects of DAMGO on striatal D1 and D2 dopamine receptor-expressing medium-sized spiny neurons. ASN NEURO 4(2):art:e00077.doi:10.1042/AN20110063

ABSTRACT

The striatum can be divided into the DLS (dorsolateral striatum) and the VMS (ventromedial striatum), which includes NAcC (nucleus accumbens core) and NAcS (nucleus accumbens shell). Here, we examined differences in electrophysiological properties of MSSNs (medium-sized spiny neurons) based on their location, expression of DA (dopamine) D1/D2 receptors and responses to the μ-opioid receptor agonist, DAMGO {[D-Ala^2-MePhe^4-Gly(ol)^5]enkephalin}. The main differences in morphological and biophysical membrane properties occurred among striatal sub-regions. MSSNs in the DLS were larger, had higher membrane capacitances and lower Rin (input resistances) compared with cells in the VMS. RMPs (resting membrane potentials) were similar among regions except for D2 cells in the NAcC, which displayed a significantly more depolarized RMP. In contrast, differences in frequency of spontaneous excitatory synaptic inputs were more prominent between cell types, with D2 cells receiving significantly more excitatory inputs than D1 cells, particularly in the VMS. Inhibitory inputs were not different between D1 and D2 cells. However, MSSNs in the VMS received more inhibitory inputs than those in the DLS. Acute application of DAMGO reduced the frequency of spontaneous excitatory and inhibitory postsynaptic currents, but the effect was greater in the VMS, in particular in the NAcS, where excitatory currents from D2 cells and inhibitory currents from D1 cells were inhibited by the largest amount. DAMGO also increased cellular excitability in the VMS, as shown by reduced threshold for evoking APs (action potentials). Together the present findings help elucidate the regional and cell-type-specific substrate of opioid actions in the striatum and point to the VMS as a critical mediator of DAMGO effects.

Key words: D1/D2 receptors, electrophysiology, nucleus accumbens, opioid receptors, striatum.

INTRODUCTION

The striatum is the principal input structure of the basal ganglia, and according to the classic anatomical perspective it can be divided into two main regions: the DLS (dorsolateral striatum) and the VMS (ventromedial striatum). The DLS mainly integrates sensorimotor information, whereas the VMS, comprising NAcC (nucleus accumbens core) and NAcS (nucleus accumbens shell), is principally involved in motivation and reward (Pennartz et al., 2009).

[1] Current address: Program in Neuroscience, Department of VCAPP, Washington State University, Wegner 205 (PO Box 646520), Pullman, WA 99164-6520, U.S.A.

[2] To whom correspondence should be addressed (email mlevine@mednet.ucla.edu).

Abbreviations: ACSF, artificial cerebrospinal fluid; AHP, after hyperpolarization; AP, action potential; AP-5, DL-2-amino-5-phosphonovaleric acid; BIC, bicuculline; CNQX, 6-cyano-7-nitroquinoxaline-2,3-dione; CsMeth, Cs-methanesulfonate; DA, dopamine; DAMGO, [D-Ala^2-MePhe^4-Gly(ol)^5]enkephalin; DLS, dorsolateral striatum; EPSC, excitatory postsynaptic current; EGFP, enhanced green fluorescent protein; IPSC, inhibitory postsynaptic current; KGluc, K-gluconate; mEPSC, miniature EPSC; mIPSC, miniature IPSC; MSSN, medium-sized spiny neuron; NAcC, nucleus accumbens core; NAcS, nucleus accumbens shell; Rin, input resistance; RMP, resting membrane potential; sEPSC, spontaneous EPSC; sIPSC, spontaneous IPSC; TBST, TBS containing 0.1% Tween 20; TTX, tetrodotoxin; UCLA, University of California at Los Angeles; VMS, ventromedial striatum; VTA, ventral tegmental area.

It is generally believed that a common neural pathway, i.e. DA (dopamine) neurons originating in the VTA (ventral tegmental area) and terminating on GABAergic MSSNs (medium-sized spiny neurons) in the NAc is involved in reward mechanisms. Drugs of abuse, such as opiates, produce reinforcing effects by modifications of the reward neuronal circuits. However, converging evidence indicates that the reinforcing actions involve both DA-dependent and DA-independent mechanisms (Pettit et al., 1984; Swerdlow et al., 1984; Hubner and Koob, 1990; Hnasko et al., 2005). Such findings suggest that, regardless of VTA involvement, reinforcing effects are mediated, at least in part, by MSSNs in the NAc.

Although the NAc has been demonstrated to be a critical component of the reward circuitry in drug abuse, the dorsal striatum is receiving more attention in addiction research (Fasano et al., 2009). The traditional dorsal and ventral divide has been challenged in favour of a dorsolateral-to-ventromedial gradient of anatomic glutamatergic and DA inputs, as well GABAergic outputs, with relevance to reinforcing behaviour (Voorn et al., 2004; Ma et al., 2009). This difference also applies to the NAc *per se*, so that there is a dorsolateral (core) to ventromedial (shell) gradient. Most addiction research has focused on one of the sub-regions of the striatum, either the DLS or the NAcC and NAcS. A complete picture of the effects of opiates, including the three sub-regions following a dorsolateral-to-ventromedial gradient, is not yet available.

Considering that more than 90% of neurons in the striatum are MSSNs, and that μ-opioid receptors are primarily involved in opiate reward, it is important to know which striatal region and cell type (DA D1 or D2 receptor-containing) play a principal role. EGFP (enhanced green fluorescent protein) has been used as a reporter gene for MSSNs expressing DA D1 and D2 receptors, which are mostly segregated into two populations of cells giving rise to the direct (D1 cells) and indirect (D2 cells) pathways. These two MSSN subtypes have distinct patterns of neuronal innervation, axonal projections and gene expression (Doig et al., 2010). Electrophysiological and anatomical evidence demonstrated important differences in morphology as well as membrane and synaptic properties of each population (Day et al., 2006, 2008; Cepeda et al., 2008; Gertler et al., 2008; André et al., 2010; Doig et al., 2010; Kravitz et al., 2010). However, most studies have concentrated on MSSNs of the dorsal striatum, and only a handful of studies have examined D1 and D2 MSSNs in ventral striatum (Kitaoka et al., 2007; Durieux et al., 2009). Although the involvement of D1 and D2 receptors has been extensively studied pharmacologically, no studies have been performed to elucidate the potential role of these two cell subpopulations in the effects of opiates.

The purpose of the present study was 2-fold; first, to examine sub-regional and cell-type-specific differences in membrane and synaptic properties of D1 and D2 receptor-containing MSSNs in DLS, NAcC and NAcS, and secondly, to determine the effects of a μ-opioid receptor agonist DAMGO {[D-Ala^2-MePhe^4-Gly(ol)^5]enkephalin}, on neuronal excitability and excitatory and inhibitory neurotransmission.

MATERIALS AND METHODS

Experimental procedures were performed in accordance with the United States Public Health Service *Guide for Care and Use of Laboratory Animals* and were approved by the Institutional Animal Care and Use Committee at the UCLA (University of California at Los Angeles). Every effort was made to minimize pain and discomfort, as well as the number of animals. Experiments were conducted on D1 ($n=41$) and D2 ($n=44$) EGFP-positive mice older than 28 days (average 42.9 ± 2.2). Details of the methodology used to generate EGFP-positive mice have been published (Gong et al., 2003) and are also available at the GENSAT web page (www.gensat.org). All mice used in the present study were heterozygous that had been back-crossed to the FVB/N background for more than 10 generations and from colonies maintained at UCLA.

Localization of MSSNs in striatal sub-regions

All the MSSNs included in this study were located within the striatum, in coronal slices taken from 1.7 to 0 mm anterior to Bregma (Franklin and Paxinos, 2007). The corpus callosum, anterior commissure and the Islands of Calleja were used as landmarks for locating the DLS, the NAcC and the NAcS. Co-ordinates for recording were as follows: DLS 1.3–0 mm anterior to Bregma, 200 μm within the dorsolateral arch of the corpus callosum; NAcC 1.3–0.8 mm anterior to Bregma, within 200 μm from the edge of the anterior commissure; NAcS 1.7–1.0 mm anterior to Bregma, ~200–500 μm medial to the anterior commissure and ~100–800 μm dorsal to the islands of Calleja (Franklin and Paxinos, 2007).

Cell visualization

EGFP-positive cells were visualized in slices using a $\times 40$ water-immersion lens on an Olympus BX50WI microscope equipped with differential interference contrast optics and fluorescence. Details for cell visualization have been described in previous papers (Cepeda et al., 2008; André et al., 2010). Once a viable MSSN in the slice was identified with IR video microscopy, the filter was switched to fluorescence mode to determine if it also was labelled with EGFP. The digitized IR image was superimposed over the fluorescence image, and electrophysiological recordings proceeded only if the cell identified with IR light showed a complete overlap with EGFP fluorescence and was in the same focal plane.

Electrophysiological recordings in slices

Whole-cell patch clamp recordings of D1 or D2 EGFP-positive MSSNs were performed using methods adapted from those

described previously (Cepeda et al., 2008). Cells also were identified by somatic size, basic membrane properties [Rin (input resistance), membrane capacitance and time constant], and by addition of biocytin (0.15%) to the internal solution. The patch pipette (3–5 MΩ) contained one of the following solutions: (i) KGluc (K-gluconate) internal solution: 140 mM KGluc, 10 mM Hepes, 2 mM $MgCl_2$, 0.1 mM $CaCl_2$, 1.1 mM EGTA and 2 mM K_2ATP, for voltage and current clamp or (ii) CsMeth (Cs-methanesulfonate) internal solution: 130 mM CsMeth, 10 mM CsCl, 4 mM NaCl, 1 mM $MgCl_2$, 5 mM MgATP, 5 mM EGTA, 10 mM Hepes, 0.5 mM GTP, 10 mM phosphocreatine and 0.1 mM leupeptin, for voltage clamp recordings (pH 7.25–7.3, osmolality, 280–290 mOsm). Access resistances were <25 MΩ. Spontaneous postsynaptic currents were recorded in standard ACSF (artificial cerebrospinal fluid) composed of the following: 130 mM NaCl, 26 mM $NaHCO_3$, 3 mM KCl, 2 mM $MgCl_2$, 1.25 mM $NaHPO_4$, 2 mM $CaCl_2$ and 10 mM glucose, pH 7.4 (osmolality, 300 mOsm). In specific experiments, sEPSCs [spontaneous EPSCs (excitatory postsynaptic currents)] were recorded in the presence of the $GABA_A$ (γ-aminobutyric acid type A) receptor antagonist, BIC (bicuculline; 20 μM) in the external solution, and by holding the membrane at −70 mV; sIPSCs [spontaneous IPSCs (inhibitory postsynaptic currents)] were recorded in the presence of NMDA (*N*-methyl-D-aspartate) and AMPA (α-amino-3-hydroxy-5-methylisoxazole-4-propionic acid) receptor antagonists AP-5 (DL-2-amino-5-phosphonovaleric acid; 50 μM) and CNQX (6-cyano-7-nitroquinoxaline-2,3-dione; 10 μM), and by holding the membrane at +10 mV. mEPSCs (miniature EPSCs) and IPSCs were recorded after addition of TTX (tetrodotoxin; 1 μM).

Recordings with KGluc internal solution

Cells were patched in voltage clamp mode and held at −70 mV. Cell membrane capacitance (in pF) was determined by applying a depolarizing step voltage command (10 mV) and using the membrane test function integrated in the pClamp8 software (Axon Instruments). This function calculates cell membrane capacitance by dividing the total charge by the voltage change. Then recordings were switched to current clamp and other parameters were determined following published methods (Heng et al., 2008). The RMP (resting membrane potential) was measured 5 min after the seal was ruptured. The *I–V* (current–voltage) relationship, used to calculate inward rectification at hyperpolarized membrane potentials, was obtained by injection of 500 ms pulses (−300 to +50 pA in 50 pA increments). The rheobase was determined as the minimal current to induce APs (action potentials) either with a short (3 ms) or a long duration (500 ms) pulse. The Rin was calculated from the voltage response to a hyperpolarizing current pulse (−100 pA). The membrane time constant was measured using Clampfit 8 by standard exponential fitting of the first 100 ms of the membrane voltage response to a −100 pA current pulse injection. For measurements of a single AP, a threshold was determined by differentiating the AP waveform and setting a rising rate of 10 mV/ms as the AP inflection point. The AP amplitude was measured from the equipotential point of the threshold to the spike peak, while the AHP (after hyperpolarization) was measured from the equipotential point of the threshold to the antipeak of the same spike. The AP duration was measured at the point of half-amplitude of the spike. Rise time (10–90% from AP threshold-to-peak) and decay time (90–10% from AP peak-to-threshold) were also calculated.

Recordings with CsMeth internal solution

After characterizing the basic membrane properties of the neuron, sEPSCs/IPSCs or mEPSCs/IPSCs were recorded for 3–6 min. The membrane current was filtered at 1 kHz and digitized at 200 μs using Clampex. sEPSCs/IPSCs were analysed off-line using the Mini Analysis Program (Jaejin Software). The threshold amplitude for the detection of a synaptic event (generally 6 pA for EPSCs and 10 pA for IPSCs), was adjusted to be 2–3 times above root mean square noise level. This software was also used to calculate EPSC frequency, amplitude for each synaptic event, and to construct time-frequency and inter-event interval histograms. Frequencies were expressed as number of events per second (Hz). EPSC/IPSC kinetic analysis used the Mini Analysis Program. For each cell, all events between 10 and 70 pA for sEPSCs or between 15 and 100 pA for sIPSCs were averaged to obtain rise and decay times, and half-amplitude durations.

Single-cell staining, confocal imaging and morphology measurements

Striatal slices containing biocytin-filled cells were fixed by immersion in 4% (w/v) paraformaldehyde in 0.1 M phosphate buffer, pH 7.4, for 2 h. Slices were washed three times for 5, 10 and 60 min respectively in 0.05 M TBST (TBS containing 0.1% Tween 20). Then they were incubated at 4°C overnight with Alexa Fluor® 488-conjugated streptavidin (Invitrogen; dilution 1:1000 with TBST) and washed with TBST. Images were obtained with a confocal laser scanning microscope (SP2 1P-FCS, Leica). Usually the cells were located 50–100 μm from the slice surface. The somatic area and the number of the primary/secondary dendrites were counted by a rater blind to MSSN location or expression of DA receptor subtype. Cells with less than three primary dendrites or less than one pair of secondary dendrites were excluded. The somatic area was calculated using Leica Confocal Software (version 2.61), by manually outlining the soma.

Statistics

Values in the Figures, Tables and text are presented as means ± S.E.M. Differences in mean values were assessed with Student/paired two-tailed *t* tests (two groups) or appropriate ANOVAs (multiple groups) followed by multiple comparisons

using Bonferroni *post hoc* tests. Differences between means were considered statistically significant if $P<0.05$.

RESULTS

The present study examined the electrophysiological properties and morphology of DA D1 and D2 receptor-expressing MSSNs stained with biocytin in striatal slices. Whole-cell patch clamp recordings from 255 MSSNs labelled with EGFP ($n=122$ D1 and $n=133$ D2) and 30 unlabelled MSSNs ($n=9$ from D1 EGFP mice, putative D2 cells, and $n=21$ from D2 EGFP mice, putative D1 cells) were obtained. Non-labelled cells in D1 or D2 EGFP mice showed no significant differences from EGFP-labelled cells in the D2 or D1 EGFP mice respectively. Thus, even though the sample of non-labelled cells was very small, the data from both labelled and non-labelled cells were pooled in their respective categories.

Differential properties of striatal D1 and D2 MSSNs follow a dorsolateral-to-ventromedial gradient

Differences in morphology

A subset of MSSNs labelled with biocytin ($n=35$) was selected for detailed morphological analysis based on the quality of the label and their somatic and dendritic field integrity. A dorsolateral-to-ventromedial gradient in cell morphology from the DLS to the NAcC and NAcS was observed (Figure 1A). Statistically significant differences in somatic area ($F_{2,29}=39.33$, $P<0.0001$; *post hoc* test, $P<0.01$ NAcS/NAcC versus DLS) (Figure 1B) and the number of primary ($F_{2,27}=21.18$, $P<0.0001$; *post hoc* test, $P<0.05$ NAcS/NAcC versus DLS) (Figure 1C) and secondary ($F_{2,26}=16.63$, $P<0.0001$; *post hoc* test, $P<0.05$ NAcS versus DLS) (Figure 1D) dendrites occurred. Thus, the more ventromedial cells had smaller somatic sizes and fewer dendrites. Although no cell-type-specific difference in somatic area was observed, D1 cells displayed more primary ($P<0.05$ in the DLS, *post hoc* test after significant ANOVA) and secondary ($P<0.05$ in the DLS and NAcS, *post hoc* test after significant ANOVA) dendrites compared with D2 cells in their respective sub-regions.

Differences in passive membrane properties

Supporting morphological differences, basic membrane properties using KGluc as the internal solution demonstrated a clear dorsolateral-to-ventromedial gradient with membrane capacitance being larger and Rin lower in DLS compared with VMS (Table 1). In addition to regional differences, the time constant values measured in current clamp mode were longer in D1 cells in NAcS compared with NAcC and DLS. In contrast, D2 cells in the NAcC displayed the longest time constants compared with either NAcS or DLS (Bonferroni *post hoc* tests $P<0.05$ after a significant two-way ANOVA).

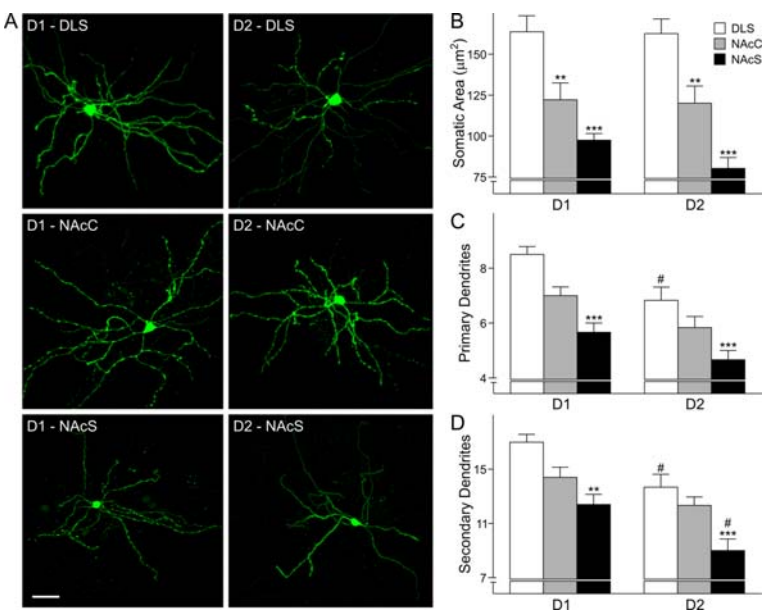

Figure 1 **Morphology of MSSNs**

(**A**) Confocal images of D1/D2 receptor-expressing MSSNs from the three sub-regions of striatum. Scale bar: 25 μm and applies to all panels. (**B–D**) Graphs show the somatic area (**B**), the number of primary (**C**) and secondary dendrites (**D**) per D1/D2 MSSN in the striatum. $n=4–6$ in each group. In this and other Figures, data are expressed as means ± S.E.M. Data were analysed by two-way ANOVA followed by Bonferroni *post hoc* test. $^{**}P<0.01$, $^{***}P<0.001$ respectively compared with DLS; $\#P<0.05$, D1 versus D2 cells in the same sub-region.

Table 1 **Basic membrane properties (KGluc internal solution)**

Data are shown as means ± S.E.M., analysed by two-way ANOVA followed by Bonferroni *post hoc* test. #$P<0.05$, ##$P<0.01$, ###$P<0.001$ respectively D1 versus D2 cells; *$P<0.05$, **$P<0.01$, ***$P<0.001$ respectively compared among striatal sub-regions.

	D1			D2		
Property	**DLS**	**NAcC**	**NAcS**	**DLS**	**NAcC**	**NAcS**
Cm (pF)	90.1 ± 6.7	77.6 ± 8.1	82.3 ± 4.5	104.1 ± 7.8	92.1 ± 8.2	75.1 ± 6.7*
Rin (MΩ)	76.1 ± 7	139.4 ± 20*	176.3 ± 21.4**	88.2 ± 15.0	200.7 ± 41.4 **	149.5 ± 8.4
Tau (ms)	5.4 ± 0.6	5.1 ± 0.5	8.7 ± 0.6***	5.2 ± 0.5	9.2 ± 1.1***, ###	6.2 ± 0.3*, #
RMP (mV)	−80.6 ± 2	−79.1 ± 1.1	−77.2 ± 0.7	−80.0 ± 1.2	−72.0 ± 1.5*, ##	−79.1 ± 1.2
I_h Amp (mV)	1.2 ± 0.2	3.5 ± 0.8*, #	2.9 ± 0.6*	1.8 ± 0.4	1.8 ± 0.2	3.1 ± 0.4*
Rheobase (pA)	928.6 ± 80	641.7 ± 83.1**	642.9 ± 41.4**	762.5 ± 55.4	460.0 ± 60*,#	542.9 ± 56.1

Differences in active membrane properties and cellular excitability

In current clamp recordings all striatal MSSNs showed hyperpolarized RMPs. There were no significant differences in RMPs except for D2 cells in the NAcC, which were significantly more depolarized (Table 1). Inward rectification, which is caused by inwardly rectifying K^+ channels, and typically observed in striatal MSSNs, was more prominent in VMS than in DLS (Figures 2A and 2B), specifically in D1 cells of the NAcS. Differences between D1 cells from NAcS and DLS were statistically significant (ANOVA repeated measures confirmed by Bonferroni *post hoc* tests, $P<0.05$). A rapid, small amplitude 'sag' (similar to the time- and voltage-dependent rectification induced by I_h), was rarely seen in MSSNs of DLS, but it became more prominent in MSSNs of VMS, except for D2 cells in the NAcC (Figure 2A, Table 1). Finally, the rheobase, which is the minimal current to evoke APs, showed a significant decrease from DLS to VMS. In general, D2 cells showed a lower rheobase compared with D1 cells, suggesting D2 cells, especially in the NAc, are more excitable (Table 1).

Differences in synaptic properties

sEPSCs were recorded at a holding membrane potential of −70 mV in the presence of BIC (20 μM). D1 cells from the NAcC/NAcS displayed reduced sEPSC frequency compared with D1 cells from DLS (Figures 3A and 3B, $P<0.0001$, Bonferroni *post hoc* test after significant differences by two-way ANOVA). In contrast, there were no differences in the frequency of D2 cells among sub-regions (Figure 3B). Within particular regions, there was a clear difference in frequency

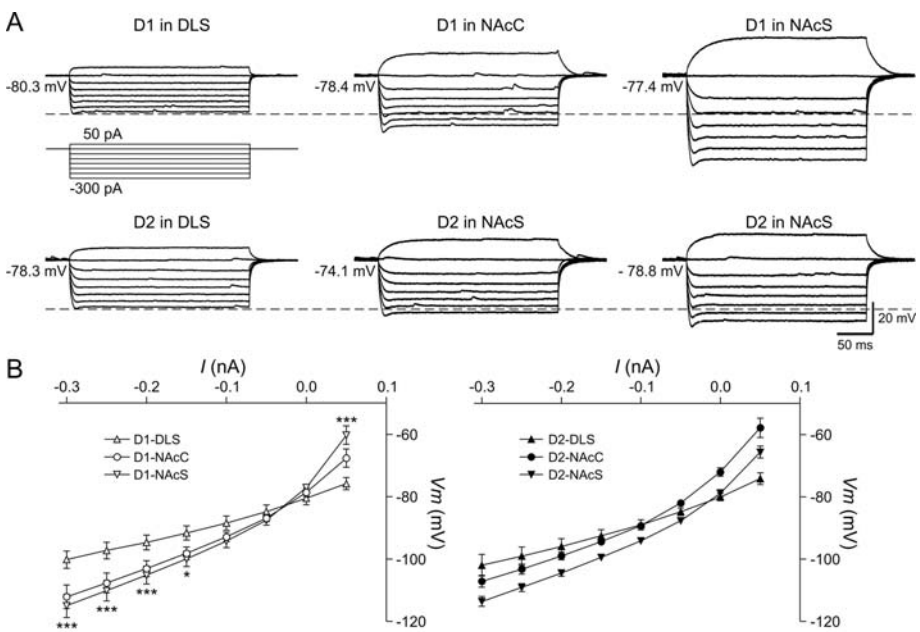

Figure 2 **Whole-cell current clamp recordings from striatal MSSNs**

(**A**) Sample traces show a gradient of inward rectification evaluated by recording responses to hyperpolarizing current steps: there is an increase from DLS to VMS (note increased voltage deflections below dashed lines in VMS compared with DLS). (**B**) *I–V* plots from groups of D1 (left panel) or D2 (right panel) receptor-expressing MSSNs, $n=9–10$ in each group. The data were analysed using ANOVA with repeated measures followed by Bonferroni *post hoc* test. *$P<0.05$, ***$P<0.001$ respectively.

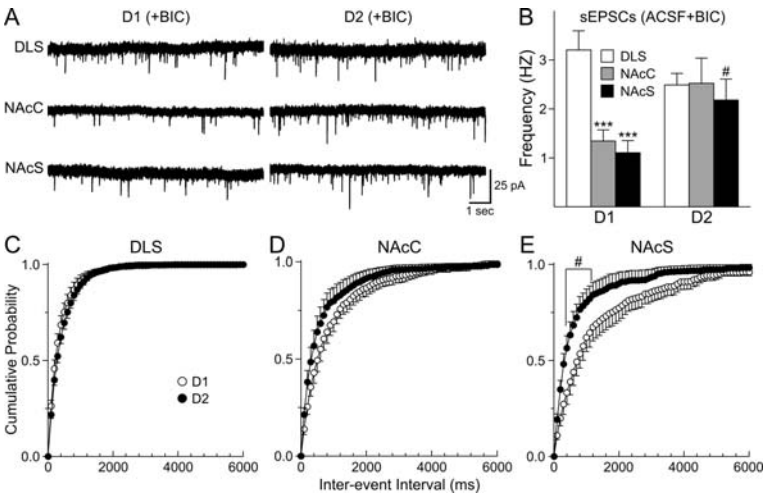

Figure 3 **Regional and cell-type-specific differences in frequency of sEPSCs in MSSNs**
(**A**) Representative traces of sEPSCs in D1/D2 cells from each sub-region (holding potential −70 mV). (**B**) Histograms show the decreased frequency of sEPSCs as well as increased differences in frequency of sEPSCs between D1 versus D2 cells in the VMS. (**C–E**) Differences of cumulative inter-event interval probability between D1 versus D2 cells in the DLS, NAcC and NAcS. For (**B–E**), n=10–13 in each group. The data were analysed using two-way ANOVA (**B**) or ANOVA with repeated measures (**C–E**) followed by Bonferroni *post hoc* tests. ***P<0.001, compared with the DLS; #P<0.05, D1 versus D2 cells.

between D1 and D2 cells from VMS but less so in cells from DLS (Figures 3C–3E). Thus, the probability of glutamate release was significantly higher in D2 compared with D1 cells in NAcC/NAcS. A significant effect of D1 versus D2 cells in the NAcC was reflected by the interaction between cell type and inter-event intervals ($F_{60,1080}$=1.81, P=0.0002) (Figure 3D). Moreover, a clear difference between D1 versus D2 cells in the NAcS was demonstrated by the effect of sub-region × cell type interaction ($F_{60,1080}$=3.86, P<0.0001), and Bonferroni *post hoc* test showed a significantly higher probability of sEPSCs in D2 cells with intervals from 400 to 900 ms (Figure 3E).

sIPSCs were isolated pharmacologically by adding AP-5 (50 μM) and CNQX (10 μM) to the external solution and by holding the membrane at +10 mV. The average frequency of sIPSCs was higher in D1 cells from the NAcC/NAcS compared with D1 cells from DLS (Figures 4A and 4B, P=0.0007, two-way ANOVA). In addition, D2 cells in the NAcS also displayed higher frequencies compared with D2 cells in the NAcC and DLS. However, contrary to the gradient of increased

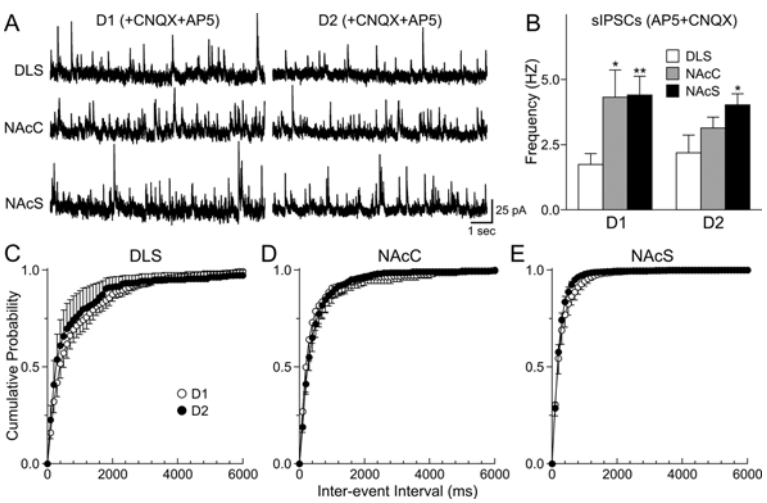

Figure 4 **Regional and cell-type-specific differences in frequency of sIPSCs in MSSNs**
(**A**) Representative traces of sIPSCs in D1/D2 cells from the DLS, NAcC and NAcS (holding potential +10 mV). (**B**) Histograms show the increased frequency of sIPSCs in the VMS compared with the DLS. (**C–E**) Show inter-event interval cumulative probabilities between D1 versus D2 cells in the DLS, NAcC and NAcS. For (**B–E**), n=9–11 in each group. The data were analysed using two-way ANOVA (**B**) or ANOVA with repeated measures (**C–E**) or followed by Bonferroni *post hoc* test. *P<0.05, **P<0.01, respectively, compared with the DLS.

differences in average sEPSC frequency between D1 and D2 cells from the DLS to the VMS, differences in sIPSC frequency between D1 and D2 cells in the striatum did not occur (Figures 4C–4E).

Differences in amplitude of sEPSCs/sIPSCs were not detected among sub-regions and between D1 versus D2 sub-types of MSSNs (data not shown). Furthermore, after addition of TTX (1 μM), neither regional nor D1/D2 subtype-dependent differences in average frequency or amplitude of mEPSC/mIPSC (miniature inhibitory postsynaptic current) were observed (data not shown). These findings suggested all the differences observed in the absence of TTX were AP-dependent.

Differential effects of DAMGO

Effects of DAMGO on excitatory synaptic transmission

The effects of the μ-opioid receptor agonist DAMGO (1 μM) on sEPSCs were evaluated 5–8 min after adding it to the ACSF and in the presence of BIC (20 μM). The effects of DAMGO on mEPSCs were determined when Na^+ currents were completely blocked by addition of TTX (1 μM). DAMGO produced a marked reduction in the frequency of sEPSCs (Figures 5A and 5B) and mEPSCs in both D1 and D2 cells from the NAcC/NAcS (at least $P<0.05$, before versus after DAMGO, by paired Student's t tests). The effects in DLS were negligible except for a significant decrease in the frequency of sEPSCs in D2 cells. Furthermore, two-way ANOVA demonstrated a significant sub-regional difference for effects of DAMGO on the average frequency of EPSCs ($F_{2,57}=7.75$, $P=0.0011$ in sEPSCs; $F_{2,\ 22}=21.84$, $P<0.0001$ in mEPSCs). Bonferroni *post hoc* tests showed significantly larger inhibitory effects of DAMGO on sEPSCs and mEPSCs in D1 cells from the NAcC/NAcS compared with the DLS. In D2 cells, the inhibitory effects of DAMGO on sEPSCs in the DLS disappeared after TTX application, whereas the effects on the NAcC/NAcS still remained (Figures 5C and 5D). The amplitudes of sEPSCs/mEPSCs were not modulated by adding DAMGO (data not shown).

Effects of DAMGO on inhibitory synaptic transmission

The effects of DAMGO on sIPSCs were examined similarly to those on sEPSCs except AP-5 (50 μM) and CNQX (10 μM) were present in the ACSF solution. Generally, DAMGO reduced the frequency of sIPSCs and mIPSCs in both D1 and D2 cells (at least $P<0.05$, before versus after DAMGO, by paired Student's t tests), except for the mIPSCs of D1 cells in the NAcS and D2 cells in the NAcC (Figures 6A and 6B). Furthermore, two-way ANOVAs demonstrated significant sub-regional differences in the effects of DAMGO on the average frequency of IPSCs ($F_{2,50}=3.60$, $P=0.0348$ in sIPSCs; $F_{2,27}=3.95$, $P=0.0312$ in mIPSCs), but no significant difference between D1 versus D2 cells ($F_{1,50}=1.13$, $P=0.2922$ in sIPSCs;

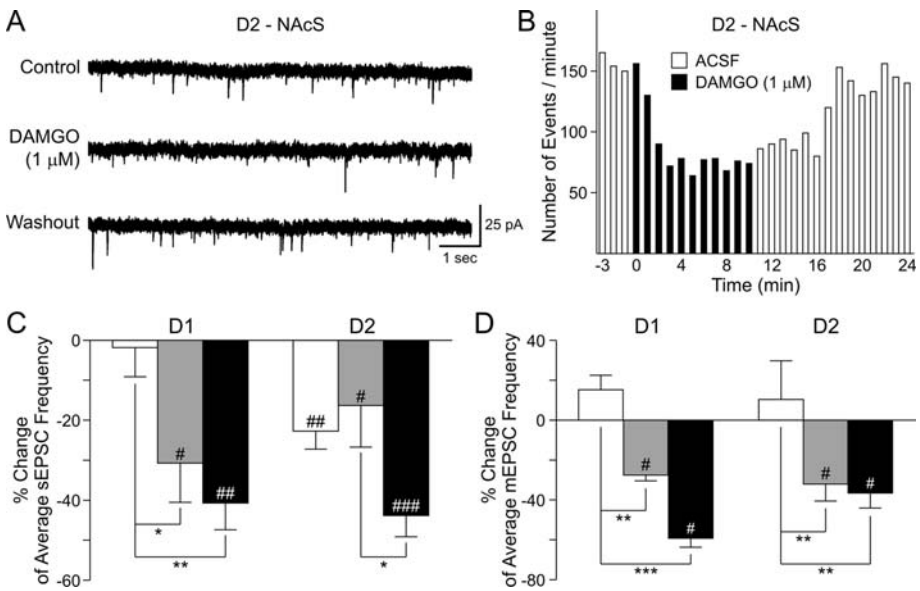

Figure 5 **Effects of DAMGO on sEPSCs in MSSNs**
(**A**) Representative recordings of sEPSCs (holding potential −70 mV) in a D2 receptor-expressing MSSN from NAcS before, during, and after washout of DAMGO (1 μM). (**B**) Representative time-course of a typical recording from another D2 receptor-expressing MSSN from NAcS before, during and after DAMGO (1 μM). DAMGO decreased the frequency of sEPSCs, which was reversed after DAMGO washout. (**C**, **D**) Histograms show the effects of DAMGO on sEPSCs (**C**) and mEPSCs (**D**) in D1/D2 cells in the DLS, NAcC and NAcS. In (**C**, **D**), data were calculated as changes of average frequencies of EPSCs during versus before DAMGO application, divided by the corresponding values before DAMGO. $n=10$–14 (**C**) or $n=5$ (**D**) in each group. The data were analysed using two-way ANOVAs followed by Bonferroni *post hoc* tests. *$P<0.05$, **$P<0.01$, ***$P<0.0001$ compared with the DLS. Also, paired t tests were performed between the average frequencies of EPSCs before versus during DAMGO application. #$P<0.05$, ##$P<0.01$, ###$P<0.001$ respectively.

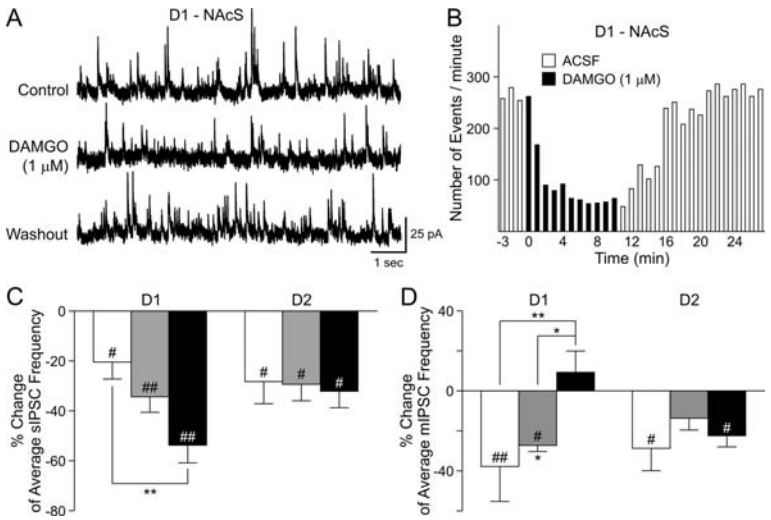

Figure 6 **Effects of DAMGO on sIPSCs in MSSNs**

(**A**) Representative traces of sIPSCs (holding potential +10 mV) in a D1 receptor-expressing MSSN from NAcS before, during and after washout of DAMGO (1 μM). (**B**) Typical time-course of a representative recording from another D1 receptor-expressing MSSN from NAcS before, during and after DAMGO (1 μM). DAMGO decreased the frequency of sIPSCs, which recovered after DAMGO washout. Histograms in (**C**, **D**) show the effects of DAMGO on sIPSCs (**C**) and mIPSCs (**D**) in D1/D2 cells in the striatum. In (**C**, **D**), data were calculated as described in Figure 5. n=8–10 (**C**) or n=5 (**D**) in each group. The data were analysed using two-way ANOVAs followed by Bonferroni *post hoc* tests. *P<0.05, **P<0.01 respectively compared with the DLS or NAcC. Also, paired t tests were performed between the average frequencies of IPSCs before versus after DAMGO. #P<0.05, ##P<0.01 respectively.

$F_{1,27}$=0.14, P=0.7072 in mIPSCs). Bonferroni *post hoc* tests showed a statistically significant increase of inhibitory effects on sIPSCs of D1, but not D2 cells in the NAcS compared with the DLS. In contrast, the sub-regional difference among the inhibitory effects on mIPSCs of D1 cells in the NAcS was significantly lower than in the DLS and the NAcC (Figures 6C and 6D). The amplitudes of sIPSCs/mIPSCs were not modulated by adding DAMGO (data not shown). In contrast, in the presence of DAMGO, sIPSCs had significantly slower kinetics, (i.e. increased decay time and half-amplitude duration) in D1 cells from NAcC and NAcS and in D2 cells from DLS and NAcC (two-way ANOVA followed by Bonferroni *post hoc* test, P<0.05 to 0.01).

Effects of DAMGO on cellular excitability

DAMGO induced a small but significant depolarization of D1 cells in the NAcC/NAcS (before versus after DAMGO, t_7=2.711, P<0.05 in the NAcC; t_7=2.541, P<0.05 in the NAcS), although no changes in the threshold for APs were detected. In contrast, no changes of RMPs in D2 cells were observed (before versus after DAMGO, t_6=1.082, P>0.05 in the NAcC; t_7=0.3917, P>0.05 in the NAcS), but the thresholds for AP generation were significantly more hyperpolarized in D2 cells (before versus after DAMGO, t_5=4.108, P<0.05 in the NAcC; t_7=2.747, P<0.05 in the NAcS), indicating increased excitability (Figure 7A, Table 2).

Both D1 and D2 cells in the NAcC/NAcS showed decreased amplitudes of AHPs (before versus after DAMGO, t_6=2.576, P<0.05, D1 cells in the NAcC; t_5=5.257, P<0.01, D1 cells in the NAcS; t_5=3.013, P<0.05, D2 cells in the NAcC), except for D2 cells in the NAcS (before versus after DAMGO, t_7=1.230, P>0.05) (Figure 7B). Furthermore, the rheobase of D1 cells in the NAcS also was significantly decreased (before versus after DAMGO, t_6=2.739, P<0.05) (Figure 7C). This evidence supports the general excitatory effects of DAMGO on intrinsic excitability of D1 and D2 MSSNs in the NAcC/NAcS (Table 2).

However, the effects of DAMGO on cellular excitability of D1 and D2 MSSNs in the DLS were not consistently changed based on assessment of different measures (summarized in Table 2). DAMGO increased Rin in D1 cells from DLS (Figure 8A, before versus after DAMGO, t_7=2.608, P<0.05), but a rightward shift of the current–response curve was seen after DAMGO treatment and the number of spikes induced by 400–500 pA current steps was reduced significantly (Figures 8B and 8C, P<0.05 at least, Bonferroni *post hoc* tests after significant two-way ANOVA with repeated measures). This indicates that the decrease in the number of spikes is not due to a reduction in Rin as an increase in this measure would predict more excitability, not less. Thus, DAMGO could be modulating different ionic conductances, e.g. Na^+, K^+ and Ca^{2+}, to decrease the number of spikes. A rightward shift of the current–response curve (P<0.05, before versus after DAMGO, significant ANOVA with repeated measures) and increased rheobase of D2 cells in the DLS indicated inhibitory effects of DAMGO, whereas the decreased amplitude of the AHP (before versus after DAMGO, t_5=3.207, P<0.05) suggested a probable increase in cellular excitability of D2 cells in the DLS (Figure 7B).

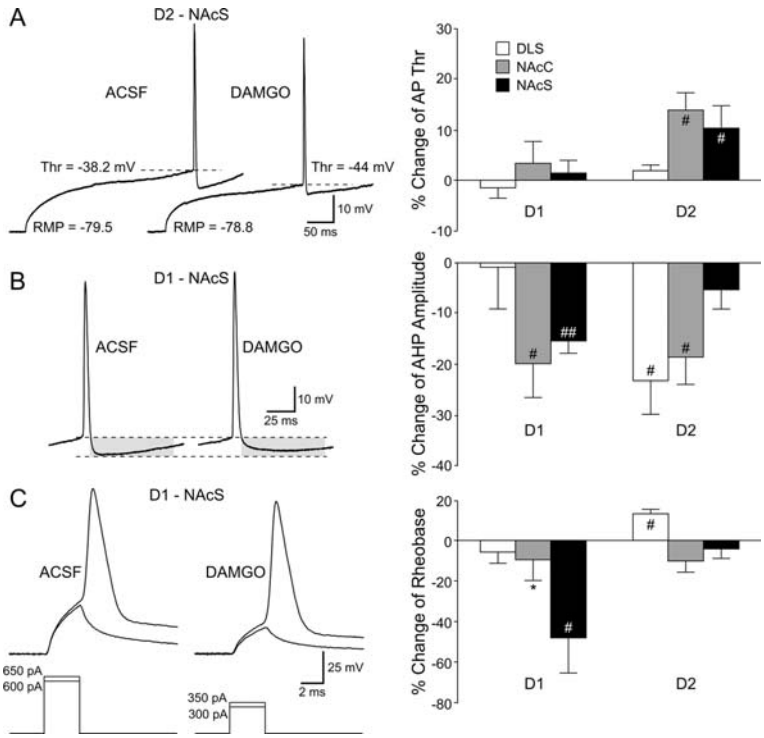

Figure 7 **Effects of DAMGO on the intrinsic excitability of MSSNs in the NAcC/NAcS**
(**A**) Representative traces (left panel) show that DAMGO decreased the AP threshold of D2 cells in NAcS. Effects of DAMGO on AP threshold of D1/D2 cells in the striatum are shown in the histograms (right panel). (**B**) Representative traces show that DAMGO decreased AHP amplitude of D1 cells in the NAcS. Effects of DAMGO on AHP amplitude of D1/D2 cells in the striatum are shown in the histograms. (**C**) Representative traces show that DAMGO decreased the rheobase of D1 cells in NAcS. Effects of DAMGO on rheobase of D1/D2 cells in the striatum are shown in the histograms. $n=5$–7 cells in each group. Data were calculated by changes of the value before versus during DAMGO application, divided by the corresponding values before DAMGO; analysed by two-way ANOVAs followed by Bonferroni *post hoc* tests, $^{*}P<0.05$, $^{**}P<0.01$, compared with the DLS. Also, paired *t* tests were performed between the average frequencies of IPSCs before versus during DAMGO in (**C**, **D**); $\#P<0.05$, $\#\#P<0.01$, respectively.

In current clamp mode (KGluc internal solution), effects of DAMGO on the kinetics of APs were observed only in the NAcC/NAcS, but not in the DLS; decay time, along with half-amplitude duration of APs of D1 cells in the NAcC/NAcS were prolonged, whereas in D2 cells they were shortened significantly (data not shown).

DISCUSSION

The present study is the first systematic comparison of D1 and D2 cells in different sub-regions of the striatum. The main findings are that the morphology, basic membrane and

Table 2 **Effects of DAMGO on intrinsic cellular excitability**
Data are shown as means ± S.E.M., analysed by paired *t* tests. $^{*}P<0.05$, $^{**}P<0.01$ respectively before versus after DAMGO.

		D1		D2	
Measurement	**Region**	**Control**	**DAMGO**	**Control**	**DAMGO**
RMP (mV)	DLS	−80.6 ± 2.0	−80.3 ± 2.6	−80.0 ± 1.2	−80.1 ± 2.4
	NAcC	−79.1 ± 1.1	−76.0 ± 1.7*	−72.0 ± 1.5	−74.3 ± 1.6
	NAcS	−77.2 ± 0.7	−65.3 ± 4.8*	−79.1 ± 1.2	−78.6 ± 2.2
AP Thr (mV)	DLS	−39.8 ± 1.8	−40.7 ± 1.9	−41.3 ± 1.1	−43.6 ± 2.5
	NAcC	−33.5 ± 2.8	−33.3 ± 4.4	−40.1 ± 0.5	−45.6 ± 1.4*
	NAcS	−35.0 ± 1.0	−35.1 ± 1.7	−36.7 ± 1.3	−38.4 ± 0.9*
AHP Amp (mV)	DLS	−9.2 ± 1.0	−8.9 ± 0.7	−10.3 ± 0.9	−8.4 ± 0.5*
	NAcC	−10.6 ± 1.1	−8.5 ± 1.2*	−10.4 ± 1.0	−8.3 ± 0.7*
	NAcS	−11.0 ± 1.4	−9.3 ± 1.3**	−9.5 ± 0.8	−9.0 ± 0.9
Rheobase (pA)	DLS	928.6 ± 80.0	885.7 ± 103.3	762.5 ± 55.4	825.0 ± 52.0*
	NAcC	641.7 ± 83.1	610.0 ± 108.9	460.0 ± 60.0	430.0 ± 102.0
	NAcS	642.9 ± 41.4	370.0 ± 34.1*	542.9 ± 56.1	578.6 ± 68.0

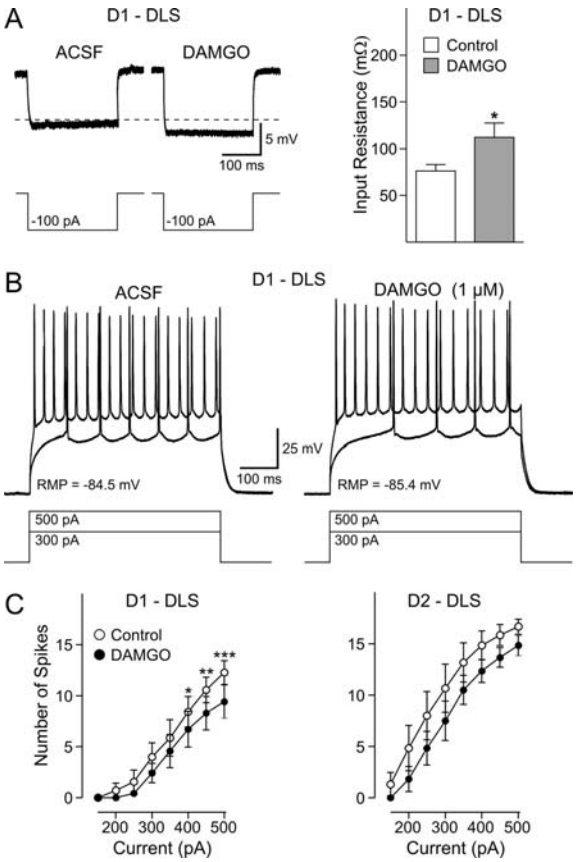

Figure 8 Effects of DAMGO on the intrinsic excitability of MSSNs in the DLS

(**A**) Representative traces and histograms show that DAMGO increased the membrane Rin of D1 cells in DLS, recorded in current clamp mode and calculated from the voltage response to a hyperpolarizing current pulse (−100 pA). (**B**) Representative traces show that DAMGO decreased firing of a D1 MSSNs in DLS; (**C**) DAMGO caused a rightward shift in the current–response curve of D1 and D2 MSSNs in DLS. $n=7$ in each group. Data are expressed as means ± S.E.M., and analysed using ANOVA with repeated measures (**A**) and paired t test (**B**); *$P<0.05$, **$P<0.01$, ***$P<0.001$ respectively compared with the control value before DAMGO application.

synaptic properties of MSSNs are differential according to a dorsolateral-to-ventromedial gradient and that the effects of the μ-opioid agonist DAMGO are more pronounced in the VMS, providing evidence that this region is the more likely anatomical substrate for the addictive properties of opiates.

Differential electrophysiological properties of striatal MSSNs

In terms of biophysical membrane properties, the present findings demonstrated a significant sub-regional gradient from DLS to NAcC and NAcS, whereby the cell capacitance decreased and the Rin increased, consistent with morphological findings that somatic size and the number of primary/secondary dendrites of MSSNs decreases from DLS to VMS. In addition, and probably as a consequence of increased Rin, MSSNs in the VMS displayed increased inward and time-dependent rectification, whereas the rheobase was reduced, suggesting higher tonic intrinsic excitability of MSSNs in the VMS compared with the DLS. The demonstration of regional differences in neuronal excitability between DLS and VMS represented by differences in Rin and rheobase, suggests that excitatory inputs to the VMS will lead to cell firing more readily than in the DLS. In agreement, previous studies comparing Rin of MSSNs from NAc and dorsal striatum found that the Rin of NAcS neurons were much higher and they fired more frequently than those in the dorsal striatum (Hopf et al., 2010).

Differences in basic membrane properties between D1 and D2 receptor-expressing MSSNs within each sub-region were more subtle than between sub-regions. Previous studies comparing basic electrophysiological properties of D1 and D2 cells in DLS have been contradictory. While some studies did not find significant differences between D1 and D2 cells (Cepeda et al., 2008; Flores-Barrera et al., 2010), others reported significantly more depolarized cell RMPs and higher Rin in D2 cells (Gertler et al., 2008). The reason for this discrepancy could be related to variations in recording sites and the dorsolateral-to-ventromedial gradient demonstrated in the present study. Nevertheless, differences occurred particularly in the VMS. The observation that D2 cells in the NAcC have the lowest rheobase, in conjunction with more depolarized RMPs, makes these cells the most excitable of the entire striatum and probably the most susceptible to changes induced by rewarding stimulation.

In terms of synaptic inputs, significant differences between D1 versus D2 cells were found, but these differences were more pronounced for sEPSCs in the VMS. Thus, in the DLS, D1 and D2 cells displayed similar frequency of sEPSCs, while in VMS D1 cells received significantly less excitatory inputs than D2 cells (more so in NAcS than in NAcC). This suggests reduced excitatory connections, possibly derived from cortical regions, on to D1 cells. Previous studies on differences in synaptic inputs between D1 and D2 cells in the DLS have been inconclusive, with studies finding no differences (Day et al., 2008), to studies finding significant differences (Cepeda et al., 2008; Kreitzer and Malenka, 2008; André et al., 2010, 2011). Several factors could explain this discrepancy, including, among others, age of mice, recording site, sample size and presence or absence of TTX. More importantly, as the present study shows, synaptic activity levels follow a dorsolateral-to-ventromedial gradient, i.e. synaptic differences are more marked in VMS, particularly in NAcS.

The DLS receives glutamatergic inputs from sensorimotor cortex, dorsal anterior cingulate cortex and dorsal prelimbic cortex, while the VMS is innervated by the ventral prelimbic and the infralimbic cortices. Considering that the regional and cell-type-specific differences of excitatory inputs disappeared when TTX was added, firing from presynaptic glutamatergic terminals is likely responsible for these differences. Why D1 cells in the VMS appear to receive less excitatory inputs remains to be elucidated, but it could mean that cortical pyramidal neurons projecting to the VMS

fire less than those projecting to the DLS. Alternatively, inputs to the VMS could be subjected to increased regulation by presynaptic D1 receptors (Pennartz et al., 1992).

In contrast, sIPSC frequency was increased in VMS. These differences were AP-dependent, as addition of TTX abolished the differences. Furthermore, we also found that these differences were cell-type-specific, so that D1 cells from the NAcC/NAcS and D2 cells in the NAcS had increased frequencies of sIPSCs compared with D1 and D2 cells in the DLS respectively. In contrast with sEPSCs, the source of inhibitory inputs is only from local circuits, including the collateral connections between striatal MSSNs and synaptic connections from GABAergic interneurons (Taverna et al., 2008). Our data suggest a higher firing rate of interneurons in the VMS, compounded with increased intrinsic excitability of MSSNs. However, the contribution of collateral connections between MSSNs to the increased sIPSCs in the VMS cannot be ruled out. Moreover, the fact that more sIPSCs were observed in the VMS compared with DLS could be associated with the suggestion of increased connectivity of cortical pyramidal neurons with fast-spiking interneurons in the VMS, which are principally entrained by high frequency oscillations in the piriform cortex, particularly after rewards (Berke, 2009).

Effects of DAMGO

In the present study, DAMGO produced differential effects on synaptic activity and intrinsic excitability, and these effects were more pronounced in VMS compared with DLS. One possibility is that sub-regional differences are related to the relative density of μ-opioid receptors throughout the striatum. The patch compartment is identified by high density of μ-opioid receptors as well as enriched enkephalin and substance P (Pert et al., 1976), while the matrix compartment has high acetylcholinesterase density but is low in μ-opioid receptors (Graybiel et al., 1981). This compartmental organization in the striatum is supported by strong evidence in the DLS (Gerfen, 1984) and the NAcC in rodents (Jongen-Relo et al., 1993), but it has been difficult to extend this regional gradient to the organization of the NAcS (Jongen-Relo et al., 1993). A higher density of patches in the anteromedial compared with the posterolateral caudoputamen was shown in a series of *in vitro* superfusion studies demonstrating that these regions in the rat differed in their sensitivities to the inhibitory regulation of opioid receptor ligands (Krebs et al., 1991, 1993, 1994). Another study provided evidence that the patches around the anterior commissure were enriched and larger compared with those in the DLS (Jongen-Relo et al., 1993).

Considering the general dorsolateral-to-ventromedial gradient (Voorn et al., 2004), we hypothesized that the distribution of μ-opioid receptors, used to identify the patch compartment, followed such a gradient in the entire striatum. This was supported by the present data demonstrating that the effects of DAMGO on both sEPSCs and sIPSCs were significantly greater in VMS than in DLS. The present study has the limitation that we did not identify MSSNs located in the patch versus the matrix compartments. However, a study found that although corticostriatal EPSCs were inhibited by μ-opioid receptors to a similar extent in the two compartments, inhibition of IPSCs by μ-opioid receptor activation was observed only in the patch compartment (Miura et al., 2007).

Our study demonstrated general inhibitory effects of DAMGO on both sEPSCs and sIPSCs, similar to previous studies demonstrating that both DA and the psychostimulant amphetamine, depress both excitatory and inhibitory synaptic transmission of MSSNs in the striatum, especially in the NAcC/NAcS (Nicola et al., 1996; Nicola and Malenka, 1997). Thus, we can hypothesize that inhibition of both excitatory and inhibitory synaptic activity is required to modify information processing by striatal MSSNs as a common response to drugs of abuse (Johnson et al., 1983; Rolls et al., 1984).

Negative regulation of both excitatory and inhibitory inputs, with a few exceptions, appeared to be mainly presynaptic as changes of frequency persisted after TTX, and kinetics, for the most part, were unchanged. In contrast, DAMGO increased intrinsic excitability of MSSNs. Both effects were stronger in VMS compared with DLS. Inhibition of synaptic inputs and increased intrinsic excitability of striatal MSSNs by activation of μ-opioid receptors could increase the signal-to-noise ratio in output neurons from the NAcC/NAcS in the striatum and affect information processing. Removal of inhibition could also facilitate increased output from VMS. Thus, acute opioid treatment could generate an integrated output in striatal MSSNs by dual inhibition of spontaneous excitatory and inhibitory synaptic transmissions and increased output.

More studies will be necessary to determine the exact roles of D1 and D2 receptor-expressing neurons in addiction behaviour (Lobo and Nestler, 2011). The present study implicates both cell types in opioid effects, as D1 and D2 cells showed increases in intrinsic excitability in VMS. However, the consequences of these changes on target output nuclei are more difficult to predict. Recent studies using selective ablation of D2 cells in the VMS showed that lack of D2 cells increased amphetamine-induced conditioned place preference. Thus, D2 striatopallidal neurons appear to limit drug reinforcement (Durieux et al., 2009). By extension, it can be suggested that D1 cells facilitate drug reinforcement and addiction (Lee et al., 2006), similar to the general plan of motor behaviour regulation by the DLS.

ACKNOWLEDGEMENTS

We thank Donna Crandall for help with the illustrations.

FUNDING

This work was supported by the USPHS (United States Public Health Service) [grant numbers NS33538 (to M.S.L.) and DA005010] and The Shirley and Stefan Hatos Foundation (to C.J.E.).

REFERENCES

André VM, Cepeda C, Cummings DM, Jocoy EL, Fisher YE, William Yang X, Levine MS (2010) Dopamine modulation of excitatory currents in the striatum is dictated by the expression of D1 or D2 receptors and modified by endocannabinoids. Eur J Neurosci 31:14–28.

André VM, Cepeda C, Fisher YE, Huynh M, Bardakjian N, Singh S, Yang XW, Levine MS (2011) Differential electrophysiological changes in striatal output neurons in Huntington's disease. J Neurosci 31:1170–1182.

Berke JD (2009) Fast oscillations in cortical-striatal networks switch frequency following rewarding events and stimulant drugs. Eur J Neurosci 30:848–859.

Cepeda C, Andre VM, Yamazaki I, Wu N, Kleiman-Weiner M, Levine MS (2008) Differential electrophysiological properties of dopamine D1 and D2 receptor-containing striatal medium-sized spiny neurons. Eur J Neurosci 27:671–682.

Day M, Wang Z, Ding J, An X, Ingham CA, Shering AF, Wokosin D, Ilijic E, Sun Z, Sampson AR, Mugnaini E, Deutch AY, Sesack SR, Arbuthnott GW, Surmeier DJ (2006) Selective elimination of glutamatergic synapses on striatopallidal neurons in Parkinson disease models. Nat Neurosci 9:251–259.

Day M, Wokosin D, Plotkin JL, Tian X, Surmeier DJ (2008) Differential excitability and modulation of striatal medium spiny neuron dendrites. J Neurosci 28:11603–11614.

Doig NM, Moss J, Bolam JP (2010) Cortical and thalamic innervation of direct and indirect pathway medium-sized spiny neurons in mouse striatum. J Neurosci 30:14610–14618.

Durieux PF, Bearzatto B, Guiducci S, Buch T, Waisman A, Zoli M, Schiffmann SN, de Kerchove d'Exaerde A (2009) D2R striatopallidal neurons inhibit both locomotor and drug reward processes. Nat Neurosci 12:393–395.

Fasano S, Pittenger C, Brambilla R (2009) Inhibition of CREB activity in the dorsal portion of the striatum potentiates behavioral responses to drugs of abuse. Front Behav Neurosci 3:29.

Flores-Barrera E, Vizcarra-Chacon BJ, Tapia D, Bargas J, Galarraga E (2010) Different corticostriatal integration in spiny projection neurons from direct and indirect pathways. Front Syst Neurosci 4:15.

Franklin KBJ, Paxinos G (2007) The Mouse Brain in Stereotaxic Coordinates, 3rd edn, Academic Press.

Gerfen CR (1984) The neostriatal mosaic: compartmentalization of corticostriatal input and striatonigral output systems. Nature 311:461–464.

Gertler TS, Chan CS, Surmeier DJ (2008) Dichotomous anatomical properties of adult striatal medium spiny neurons. J Neurosci 28:10814–10824.

Gong S, Zheng C, Doughty ML, Losos K, Didkovsky N, Schambra UB, Nowak NJ, Joyner A, Leblanc G, Hatten ME, Heintz N (2003) A gene expression atlas of the central nervous system based on bacterial artificial chromosomes. Nature 425:917–925.

Graybiel AM, Ragsdale CW Jr, Yoneoka ES, Elde RP (1981) An immunohistochemical study of enkephalins and other neuropeptides in the striatum of the cat with evidence that the opiate peptides are arranged to form mosaic patterns in register with the striosomal compartments visible by acetylcholinesterase staining. Neuroscience 6:377–397.

Heng LJ, Yang J, Liu YH, Wang WT, Hu SJ, Gao GD (2008) Repeated morphine exposure decreased the nucleus accumbens excitability during short-term withdrawal. Synapse 62:775–782.

Hnasko TS, Sotak BN, Palmiter RD (2005) Morphine reward in dopamine-deficient mice. Nature 438:854–857.

Hopf FW, Seif T, Mohamedi ML, Chen BT, Bonci A (2010) The small-conductance calcium-activated potassium channel is a key modulator of firing and long-term depression in the dorsal striatum. Eur J Neurosci 31:1946–1959.

Hubner CB, Koob GF (1990) The ventral pallidum plays a role in mediating cocaine and heroin self-administration in the rat. Brain Res 508:20–29.

Johnson SW, Palmer MR, Freedman R (1983) Effects of dopamine on spontaneous and evoked activity of caudate neurons. Neuropharmacology 22:843–851.

Jongen-Relo AL, Groenewegen HJ, Voorn P (1993) Evidence for a multi-compartmental histochemical organization of the nucleus accumbens in the rat. J Comp Neurol 337:267–276.

Kitaoka S, Furuyashiki T, Nishi A, Shuto T, Koyasu S, Matsuoka T, Miyasaka M, Greengard P, Narumiya S (2007) Prostaglandin E2 acts on EP1 receptor and amplifies both dopamine D1 and D2 receptor signaling in the striatum. J Neurosci 27:12900–12907.

Kravitz AV, Freeze BS, Parker PR, Kay K, Thwin MT, Deisseroth K, Kreitzer AC (2010) Regulation of Parkinsonian motor behaviours by optogenetic control of basal ganglia circuitry. Nature 466:622–626.

Krebs MO, Trovero F, Desban M, Gauchy C, Glowinski J, Kemel ML (1991) Distinct presynaptic regulation of dopamine release through NMDA receptors in striosome- and matrix-enriched areas of the rat striatum. J Neurosci 11:1256–1262.

Krebs MO, Kemel ML, Gauchy C, Desban M, Glowinski J (1993) Local GABAergic regulation of the N-methyl-d-aspartate-evoked release of dopamine is more prominent in striosomes than in matrix of the rat striatum. Neuroscience 57:249–260.

Krebs MO, Gauchy C, Desban M, Glowinski J, Kemel ML (1994) Role of dynorphin and GABA in the inhibitory regulation of NMDA-induced dopamine release in striosome- and matrix-enriched areas of the rat striatum. J Neurosci 14:2435–2443.

Kreitzer AC, Malenka RC (2008) Striatal plasticity and basal ganglia circuit function. Neuron 60:543–554.

Lee KW, Kim Y, Kim AM, Helmin K, Nairn AC, Greengard P (2006) Cocaine-induced dendritic spine formation in D1 and D2 dopamine receptor-containing medium spiny neurons in nucleus accumbens. Proc Natl Acad Sci USA 103:3399–3404.

Lobo MK, Nestler EJ (2011) The striatal balancing act in drug addiction: distinct roles of direct and indirect pathway medium spiny neurons. Front Neuroanat 5:41.

Ma YY, Cepeda C, Cui CL (2009) The role of striatal NMDA receptors in drug addiction. Int Rev Neurobiol 89:131–146.

Miura M, Saino-Saito S, Masuda M, Kobayashi K, Aosaki T (2007) Compartment-specific modulation of GABAergic synaptic transmission by μ-opioid receptor in the mouse striatum with green fluorescent protein-expressing dopamine islands. J Neurosci 27:9721–9728.

Nicola SM, Malenka RC (1997) Dopamine depresses excitatory and inhibitory synaptic transmission by distinct mechanisms in the nucleus accumbens. J Neurosci 17:5697–5710.

Nicola SM, Kombian SB, Malenka RC (1996) Psychostimulants depress excitatory synaptic transmission in the nucleus accumbens via presynaptic D1-like dopamine receptors. J Neurosci 16:1591–1604.

Pennartz CM, Dolleman-Van der Weel MJ, Kitai ST, Lopes da Silva FH (1992) Presynaptic dopamine D1 receptors attenuate excitatory and inhibitory limbic inputs to the shell region of the rat nucleus accumbens studied *in vitro*. J Neurophysiol 67:1325–1334.

Pennartz CM, Berke JD, Graybiel AM, Ito R, Lansink CS, van der Meer M, Redish AD, Smith KS, Voorn P (2009) Corticostriatal interactions during learning, memory processing, and decision making. J Neurosci 29:12831–12838.

Pert CB, Kuhar MJ, Snyder SH (1976) Opiate receptor: autoradiographic localization in rat brain. Proc Natl Acad Sci USA 73:3729–3733.

Pettit HO, Ettenberg A, Bloom FE, Koob GF (1984) Destruction of dopamine in the nucleus accumbens selectively attenuates cocaine but not heroin self-administration in rats. Psychopharmacology (Berl) 84:167–173.

Rolls ET, Thorpe SJ, Boytim M, Szabo I, Perrett DI (1984) Responses of striatal neurons in the behaving monkey. 3. Effects of iontophoretically applied dopamine on normal responsiveness. Neuroscience 12:1201–1212.

Swerdlow NR, Swanson LW, Koob GF (1984) Electrolytic lesions of the substantia innominata and lateral preoptic area attenuate the 'super-sensitive' locomotor response to apomorphine resulting from denervation of the nucleus accumbens. Brain Res 306:141–148.

Taverna S, Ilijic E, Surmeier DJ (2008) Recurrent collateral connections of striatal medium spiny neurons are disrupted in models of Parkinson's disease. J Neurosci 28:5504–5512.

Voorn P, Vanderschuren LJ, Groenewegen HJ, Robbins TW, Pennartz CM (2004) Putting a spin on the dorsal-ventral divide of the striatum. Trends Neurosci 27:468–474.

Received 13 December 2011/accepted 24 January 2012

Published as Immediate Publication 25 January 2012, doi 10.1042/AN20110063